Journal of the European Ceramic Society **15** (1995) 71–80
© 1995 Elsevier Science Limited
Printed in Great Britain. All rights reserved
0955-2219/95/$9.50

Morphological Characterization of Hot-pressed α-SiC with Al-based Additives Deformed by Compression at High Temperature

M. L. Duval-Riviere,[a] M. Coster,[a] L. Chermant,[a] J. Vicens[a] & C. Carry[b]

[a] Lermat, URA CNRS 1317, ISMRA, 6 Bd du Maréchal Juin, 14050 Caen Cedex, France
[b] ISMA, Université Paris-Sud, Orsay, France

(Received 22 January 1994; revised version received 15 June 1994; accepted 28 June 1994)

Abstract

An automatic image analysis method has been used to study the microstructure evolution of polycrystalline α-SiC samples hot pressed with 0·3 wt% and 1·5 wt% Al-based additives after compression at high temperature. Microstructures have been characterized in terms of grain shape, grain size and grain orientation with respect to the macroscopic stress direction. It has been shown that grains tend to flatten perpendicularly to the external stress for the 0·3 wt% Al grade. By contrast, for the same macroscopic deformation value, grains of the 1·5 wt% Al grade do not exhibit any shape change after creep tests, suggesting that a certain amount of superplastic deformation has occurred.

1 Introduction

Among the thermomechanical ceramics, polycrystalline ceramics based on silicon carbide have been one of the primary candidate ceramic materials for use in structural applications at high temperature. Consequently many studies have been devoted to their mechanical behaviour in a wide range of stress and temperature.[1–16] However, many experiments were conducted in a temperature range not exceeding 1600–1700°C and/or with bending as the preferred mode of testing, so that overall strains of a few percent were reached.[1–7] In most cases, high-temperature creep in polycrystalline SiC has been interpreted in terms of diffusional atomic flow rather than in terms of dislocation glide even if a parallel dislocation glide mechanism can contribute to the total strain.[1–7] However, experiments conducted on SiC single crystals have shown that plastic strain was due to dislocation glide motion on the basal slip system and was controlled by a Peierls mechanism.[15,16] The same mechanism was found in CVD SiC deformed between 1400–1600°C.[10]

During the high-temperature thermomechanical treatments, a modification of the microstructure of the material can occur,depending on the experimental conditions as well as on the mechanism inducing the deformation. For example, grain shape modification is generally observed for dislocation and diffusional creep[17] but not during superplastic creep.[18] The change of the microstructure is usually investigated by means of image analysis methods. In SiC materials these methods were used in a few cases to characterize grain sizes and grain shapes before and after deformation.[11,12]

On the other hand, compressive tests of different grades of α-SiC sintered with Al-based additives were carried out by Carry & Mocellin beyond 1800°C in compression so that, in contrast to the preceding studies,[1–7] higher strain values could be reached (0·43) without cavitation.[8]

The aim of this work is to characterize by using image analysis methods the microstructural evolution of the α-SiC materials creep tested in conditions given in Ref. 8. Grain size and grain shape evolutions have been determined for the two grades containing 0·3 wt% Al and 1·5 wt% Al compressed at different stress values in a temperature range 1850–1950°C. The present study is a part of a more general microstructural investigation performed on several crept polycrystalline SiC materials taking into account creep parameters.

2 Materials and procedure

Two grades of commercial hot-pressed Al-doped α-SiC (Elektroschmelzwerk Company, Kempten,

Table 1. Annealing and creep parameters (following the data of Carry & Mocellin[8])

Sample numbers	*T(°C)*	*σ(MPa)*	*t(min)*	*$\|\varepsilon_f\|$*	*⟨L⟩ (μm) ± 0·2*	*$\sqrt{\bar{s}}$*	*e*	*d_1/d_2 (± 0·05)*	*$\langle L_\parallel\rangle/\langle L_\perp\rangle$*	*α(°)*
As-sintered (0·3 wt%)	—	—	—	—	—	2	—	—	0.83	—
1	1900	—	420	—	3·01	—	0·40	0·92	—	26
2	1900	45–55	420	0·250	2·86	—	0·68	0·73	—	4
				—	2·58	—	0·30	0·95	—	23
3	1950	—	395	—	—	2·50	—	—	0·90	—
	1950	45–55	395	0·428	3·12	—	0·79	0·61	—	1·5
					—	2·70	—	—	0·60	—
4 $\sigma_\parallel$	1950	45–55	395	0·428	2·32	—	0·44	0·90	—	68
4 $\sigma_\perp$										
As-sintered (1·5 wt%)	—	—	—	—	—	1·1	—	—	0·71	—
5	1900	—	200	—	1·71	—	0·72	0·69	—	77
6	1900	44–52	200	0·274	1·55	—	0·74	0·67	—	73
					—	1·60	—	—	0·70	—
7	1900	88–102	95	0·430	1·45	—	0·70	0·71	—	76
8	1850	—	147	—	—	1·3	—	—	0·90	—
9	1850	88–102	147	0·26	—	1·3	—	—	0·80	—

Results of global analysis for annealed and deformed samples are given. Mean intercept length $\langle L\rangle$, eccentricity e, d_1d_2 ratios and α are displayed for several samples.
Results obtained by the classical intercept method are also given. The mean grain size $\sqrt{\bar{s}}$ and $\langle L_\parallel\rangle/\langle L_\perp\rangle$ ratios are displayed for several samples and should be compared to $\langle L\rangle$ and d_1/d_2 ratios respectively when results are displayed for the two methods.

Germany) have been crept by compression between 1850–1950°C. Aluminium levels were 0·3 wt% and 1·5 wt%. Test samples for creep experiments were obtained by diamond cutting and machining from the as-received discs (75 mm diameter by 25 mm height). Relative positions and orientations of samples inside the original discs were recorded. Indeed, structural and chemical composition variations might be expected between the core and the outer surfaces. Results of the present work have been focused on samples located in the core of the original discs. Samples for creep experiments with dimensions $a \times a \times 3a$ ($8{\cdot}7 < a < 13$ mm) were used and smaller pieces were also cut to serve as reference samples. They were heated with the piece being creep tested. Annealing and creep parameters are given in Table 1, according to the data reported in Ref. 8. Moreover, metallographic sections, which were studied by image analysis methods, were chosen in the middle part of the high-temperature deformed specimens.

3 Image Analysis Method

Automatic image analysis was used to obtain quantitative information on the microstructure of SiC samples. Metallographic sections containing the compressive and/or the hot-pressing directions were etched by the Murakami solution (NaOH + $[Fe(CN)_6]K_3$). Then optical (Olympus BH2) and SEM micrographs (Jeol JSM T330 A) were analysed by using a texture analyser Nachet Microcontrole NS1500.

For this work, two types of morphological data are necessary: the grain size and the grain anisotropy characterized by orientation and shape indices. Before measurements, the video image was thresholded to obtain a binary image (using a top hat transformation). Then binary images were filtered by morphological and geodesical opening. This is followed by a skeletonization by influence zone denoted SKIZ.[19,20] In these conditions, white pixels belong to SiC grains and black pixels to grain boundaries. After SKIZ, the grain boundary thickness was reduced to a thickness of one pixel. After this image processing two types of analyses were used. In the first case, measurements were performed on the binary image itself (global analysis). In the second case, each grain totally included in the image field was separately measured (individual analysis).

For global analysis several parameters have to be chosen. Parameters corresponding to the grain size are obtained by mean intercept measurements by unit length denoted N_L. If V_v is the volumic ratio of the additive phase, the mean grain size $\langle L\rangle$ is given by $(1 - V_v)/N_L$, or $1/N_L$ when the intergranular phase content is negligible. Since a hexagonal lattice of pixels is used in our texture analyser NS1500, the modelization of the grain anisotropy is realized by using an equivalent ellipse associated with the grains. An algorithm given by Serra[20] allows the associated ellipse to be defined by means of parameters which have been indicated in Fig. 1. The minor and the major axes of the ellipse denoted d_1 and d_2 are related to the eccentricity value e of the ellipse following the

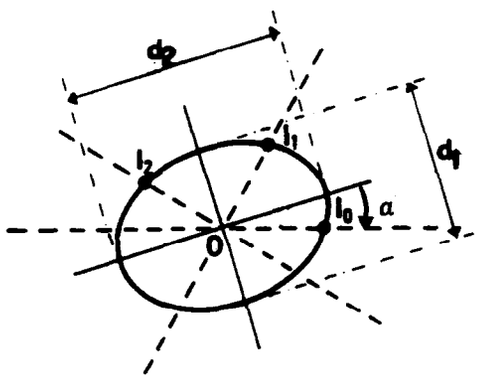

Fig. 1. Equivalent ellipse associated to the grains with its parameters.

relation:

$$e = \sqrt{1 - \frac{d_1^2}{d_2^2}} \tag{1}$$

The angle α is related to the orientation of the major axis d_2 with respect to a reference direction.

Because measurements are made in a hexagonal lattice of pixels, three intercept values N_L are determined in the three main directions (0, $\pi/3$, $2\pi/3$) (Fig. 1). Then a conic can be drawn passing through I_0, I_1 and I_2 (denoted in Fig. 1). I_0, I_1 and I_2 are expressed in a polar coordinate system. In the present case an elliptic model is always obtained.

The same type of parameters (grain size $\langle L \rangle$, eccentricity e and orientation α) have been determined by individual image analysis methods. Results are displayed either by cumulative or frequency distributions. The grain size d is given by the equivalent diameter of the surface area of each grain. The equivalent ellipse of each grain is obtained by the same algorithm as the global analysis method by using a hexagonal convex hull of each grain in order to minimize the noise of grain boundaries. By individual analysis it is possible to draw grain size and angle distributions. This information may be different from the previous one obtained by global analysis since, for example, anisotropic grains can give an isotropic texture if the grains are distributed in all directions.

This last point is illustrated in the schematic representation of Fig. 2 where anisotropic grains have been randomly orientated in Fig. 2(a). By contrast, anisotropic grains have been drawn in a preferential orientation in Fig. 2(b). In both cases (Fig. 2(a) and (b)) the individual analysis method does indicate that grains have an anisotropic shape. However, by global analysis, examples of Fig. 2(a) and (b) will be found to be isotropic and anisotropic respectively.

In parallel to this automatic method, other metallographic sections of several samples were also analysed by a classical intercept method. In this last method only average section area $\bar{s}$ and intercept values in two perpendicular directions related to the hot-pressing direction P or to the compressive stress σ are measured. Thus this method gives only two morphological parameters: the mean grain size $\sqrt{\bar{s}}$ and $\langle L_{\parallel} \rangle / \langle L_{\perp} \rangle$ ratios.

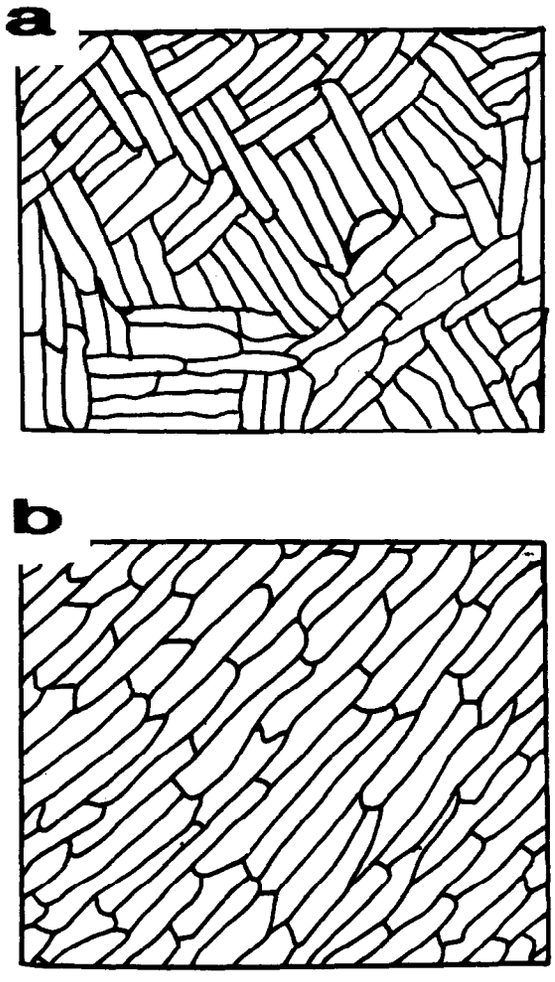

Fig. 2. Schematic representation of (a) anisotropic grains and isotropic structure; (b) anisotropic grains and anisotropic structure.

4 Results and Discussion

All specimens analysed are listed in Table 1. Two grades of SiC-Al additives samples are reported. For each grade, the as-sintered and two or three annealed samples with their deformed states have been studied. So this group is considered to be representative for the study of microstructural modifications occurring during these five creep experiments performed in a very short range of temperatures and stresses. Moreover, as shown in Table 1, results obtained from the automatic and the classical intercept methods are reported for several samples.

In Section 4.1 the main microstructural evolution is described from optical or SEM micrographs of each sample.

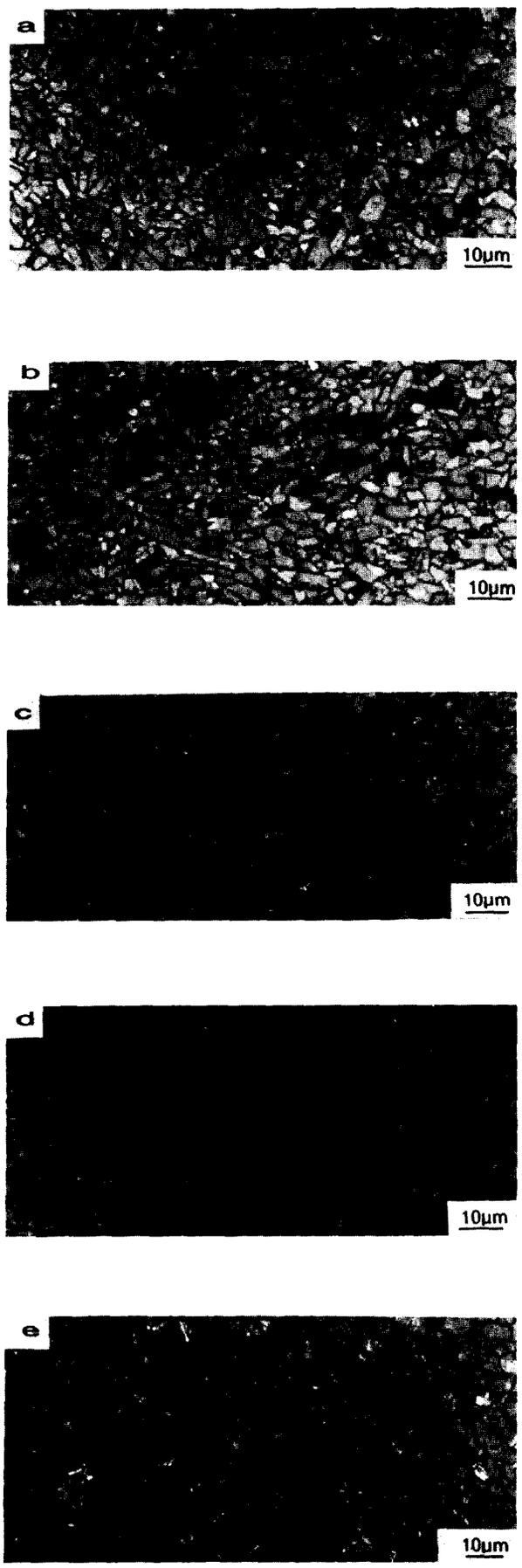

Fig. 3. Optical micrographs of the 0·3 wt% grade. (a) Sample 1 annealed at 1900°C. P is the direction of the stress acting during the sintering. (b) Sample 2 deformed with an overall strain ε_f = 0·25. The direction of the compressive stress σ is indicated. (c) Sample 3 annealed at 1950°C. (d) Sample 4 deformed with an overall strain ε_f = 0·428. (e) Same sample as in (d) but shown perpendicularly to the external stress σ.

4.1 Qualitative analyses of annealed or deformed specimens

4.1.1 Al grade (0·3 wt%)

Optical micrographs of the 0·3 wt.% Al grade are presented in Fig. 3. The two reference states (1 and 3) with their corresponding deformed specimens (2 and 4) are shown in Fig. 3(a) to (e). The hot-pressing stress direction P as well as the compressive stress direction σ have been indicated on each micrograph. Metallographic sections of deformed specimens contain the compressive stress direction σ. Moreover, a metallographic section perpendicular to σ is also given for the sample 4 (Fig. 3(e)). These optical micrographs are good enough to visualize all grain boundaries. However, in order to increase the contrast, it has been necessary to draw in dark ink all grain boundaries being acquired. The dark pockets which can be seen on these micrographs are likely to be due to the presence of the additives used during the sintering process.

In all deformed specimens, no significant grain growth could be detected by comparison with annealed samples. It appears that grains have a tendency to flatten in a direction perpendicular to the external stress σ after the compressive test (Fig. 3(b) and (d)). This is quite clear for sample 4 (Fig. 3(d)) which has the highest strain value (0·43). For the same sample the section cut perpendicularly to σ (Fig. 3(e)) shows grains with a quasi-equiaxed shape. This indicates that grains viewed in a cross-section containing σ can be probably described by an elliptic shape. Thus the large axis is located in a plane normal to σ. By contrast, no preferential orientation of the grains with respect to P is clearly visible in the reference state 3 (Fig. 3(c)). However, grains appear slightly elongated in a direction perpendicular to P (sample 1, Fig. 3(a)).

4.1.2. Al grade (1·5 wt.%)

For this grade the optical method was not suitable because the grain size is twice as small as the grain size of the 0·3 wt.% Al grade. Thus the SEM method was chosen. Micrographs of samples 5, 6 and 7 are given in Fig. 4(a)–(c). The reference state (5) is displayed in Fig. 4(a) and the two deformed samples (6 and 7) in Fig. 4(b) and (c).

Compared to the other grade (0.3 wt.%), it seems that no grain shape modification has appeared in the two deformed samples even for sample 6 which has a high strain value (0·43) and has been deformed under 88–102 MPa.

4.2 Image analysis results

Qualitative results displayed in Section 4.1 have been quantified either by global or individual image analysis.

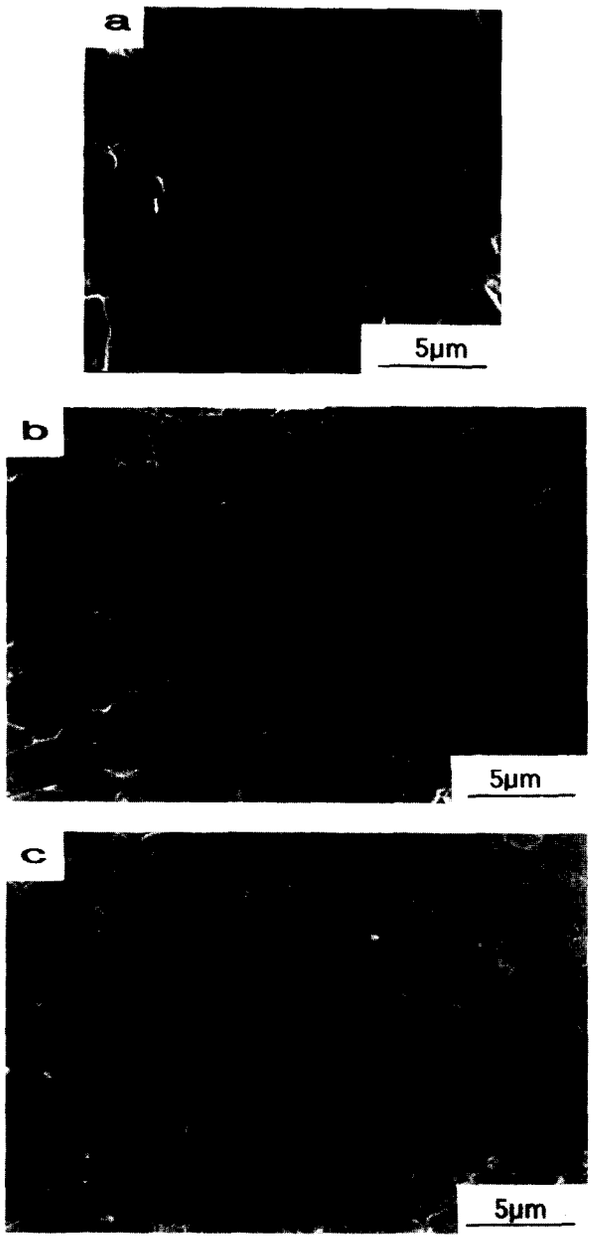

Fig. 4. SEM micrographs of the 1·5 wt% grade. (a) Sample 5 annealed at 1900°C. (b) Sample 6 deformed with an overall strain ε_f = 0·274. (c) Sample 7 deformed with an overall strain ε_f = 0·43. P and σ stress directions have been indicated on each micrograph.

4.2.1 Global analysis

Due to the two different techniques used in this work, i.e. optical and SEM, the number of analysed grains is more than 1500 for the 0·3 wt% grade and about 800 for the 1·5 wt% grade, which is enough to obtain quantitative data. Results of global and classical intercept analyses are in good agreement if $\langle L \rangle$ and d_1/d_2 ratios (global analysis) are compared with $\sqrt{s}$ and $\langle L_\parallel \rangle / \langle L_\perp \rangle$ ratios (classical intercept method) respectively (Table 1).

4.2.1.1 Al grade (0·3 wt.%). The mean grain size value is equal to ~3 μm and a very slight grain growth is observed for sample 4 (3·12 μm) compared to its reference state, sample 3 (2·58 μm).

The reference states (samples 1 and 3) are equivalent in terms of eccentricity and correspond to a quasi-equiaxed structure with d_1/d_2 ratios close to 0·9. For the two deformed specimens, d_1/d_2 ratios deduced from the eccentricity values are 0·73 (sample 2) and 0·61 (sample 4). As a comparison, a ratio d_1/d_2 equal to 0·5 corresponds to an eccentricity value of 0·86. For the reference states (samples 1 and 3) the α values do not indicate a clear preferential orientation with respect to the hot-pressing stress. By contrast, it is clearly demonstrated that, as previously suggested on the micrographs, deformed grains tend to align perpendicularly to σ (α = 1·5° (sample 4) and α = 4° (sample 2)). Consequently the minor axis of the equivalent ellipse denoted d_1 is found to be parallel to the external stress. Thus, in the following, d_1 and d_2 are denoted $d_\parallel$ and $d_\perp$ respectively.

Moreover, if grain growth is negligible, it is possible to define the grain deformation ε_g by the formula

$$\varepsilon_g = \ln (d_\parallel / d_0) \tag{2}$$

where $d_\parallel$ and d_0 are respectively the diameter parallel to the external stress and the grain diameter of the undeformed specimen.[21]

If the volume of grains remains constant before and after the grain deformation, the relation between $d_\parallel$ and $d_\perp$ and d_0 can be written $d_\parallel \cdot d_\perp^2 = d_0^3$. Then the grain deformation ε_g becomes

$$\varepsilon_g = 2/3 \ln (d_\parallel / d_\perp) \tag{3}$$

Grain, deformation is theoretically calculated from a quasi-equiaxed initial shape. Because grains are slightly elongated in the as-sintered state, the calculation underestimates the grain deformation.

Grain deformation ε_g and the total strain of the sample ε_f values are reported in Fig. 5 (samples 2 and 4). This curve shows that grains follow approximately the same shape change as the sample at the macroscopic level. Thus the slight grain growth observed for samples 2 and 4 (Table 1) does not affect the result shown in Fig. 5.

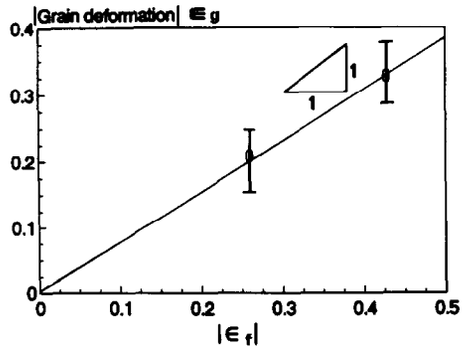

Fig. 5. Evolution of the grain deformation ε_g with the overall deformation of the sample ε_f : ε_g = 2/3 ln ($d_\parallel/d_\perp$).

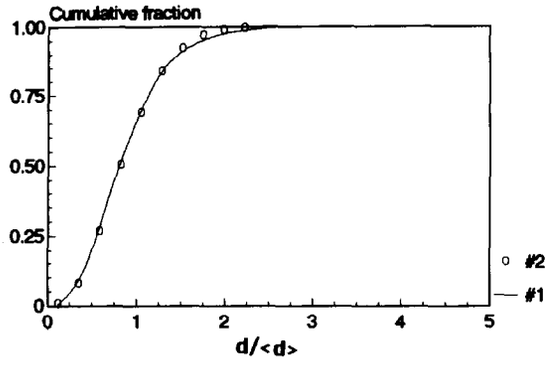

(a)

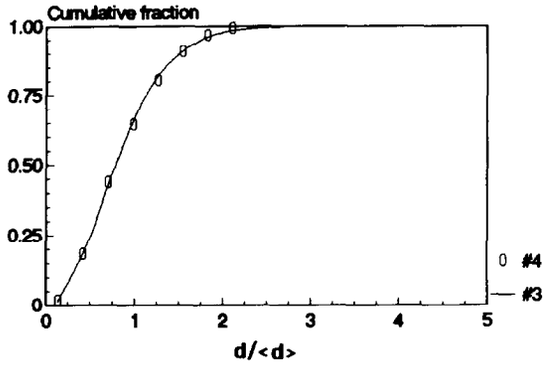

(b)

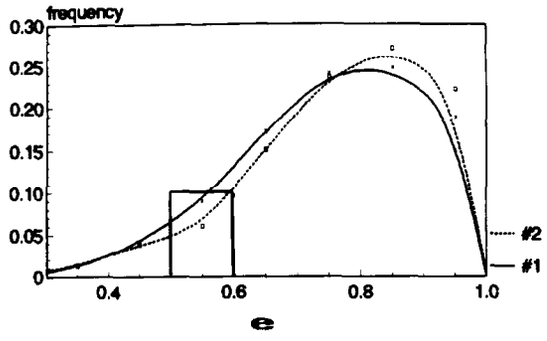

(c)

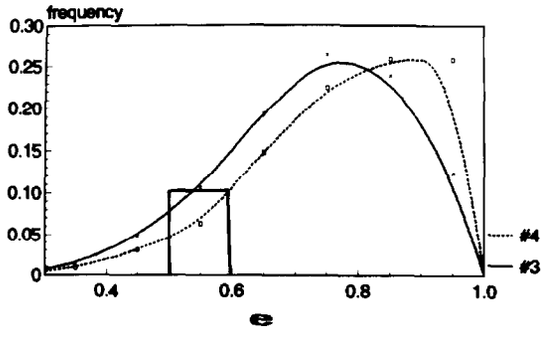

(d)

Fig. 6. Cumulative fractions of the normalised equivalent grain diameter $d/\langle d\rangle$ for (a) samples 1 and 2 and (b) for samples 3 and 4. Frequency distributions of the eccentricity e (c) for samples 1 and 2 and (d) for samples 3 and 4. The value of the class used in these frequency distributions has been drawn in (c) and (d).

4.2.1.2 Al grade (1·5 wt%). For this grade, the grain size of annealed and deformed specimens is found to be close to 1·5 μm. The reference state (sample 5) exhibits an anisotropy of the grain shape in contrast to the preceding cases (samples 1 and 3). It can be noted that the deformed specimens, even the most deformed one (sample 7), have the same eccentricity values as the reference state (e ~ 0·7). Consequently the grain deformation cannot be correlated to the overall deformation of the sample. These results are in agreement with the α values, found to be nearly equivalent for the three samples (5, 6, 7). This indicates that no strong preferential orientation has occurred during the creep tests.

Finally the grain size $\langle L\rangle$ and d_1/d_2 ratios of the two grades in the as-sintered state have been found to be equal respectively to: $\langle L\rangle = 2$ μm, $\langle L_\parallel\rangle/\langle L_\perp\rangle = 0{\cdot}83$ (0·3% Al grade) and $\langle L\rangle = 1{\cdot}1$ μm, $\langle L_\parallel\rangle/\langle L_\perp\rangle = 0{\cdot}71$ (1·5 wt.% Al grade) (Table 1). By comparison with values concerning annealed samples (1, 3, 5, 8), it appears that a slight grain growth has occurred during the annealing treatments for the two grades.

4.2.2 Individual analysis

4.2.2.1 Al grade (0·3 wt%). Results concerning the grain size and the grain shape are given in Fig. 6. Cumulative fractions of the normalized equivalent grain diameter $d/\langle d\rangle$ are given in Fig. 6(a) (samples 1 and 2) and in Fig. 6(b) (samples 3 and 4). Frequency distributions of the eccentricity e are shown in Fig. 6(c) (samples 1 and 2) and in Fig. 6(d) (samples 3 and 4). The main evolutions of these two parameters (d and e) are in agreement with the results of the global analysis. Particularly, for the two deformed samples, the eccentricity values, displayed by frequency curves, are shifted towards higher values. In fact these displacements can be evaluated by the mode values for each curve. For the most deformed specimen (sample 4, Fig. 6(d)), the mode value is found to be 0·9 compared to 0·75 in the annealed state (sample 3) which is significant, taking into account the value of the class of the distribution curve (0·1), indicated on Fig. 6(c) and (d). Therefore the slight variation of the mode found for samples 1 and 2 (0·80 to 0·85) is less significant. On the other hand, the cumulative curves of grain size distribution are close to a normal logarithmic law and seem not to be affected by thermomechanical treatments.

Moreover, the distribution of α values is displayed in Fig. 7 for the four samples. A difference is visible between the distribution curves of references (samples 1 and 3, Fig. 7(a) and (b)) and deformed states (samples 2 and 4, Fig. 7(c) and (d)).

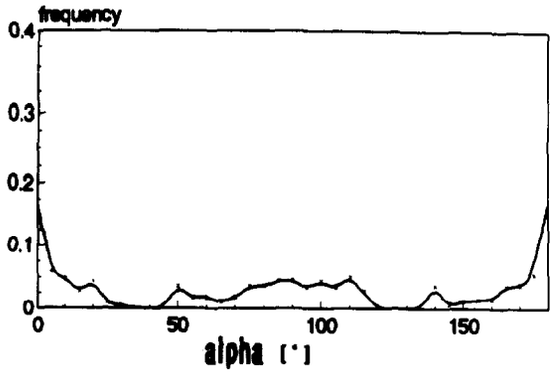

(a)

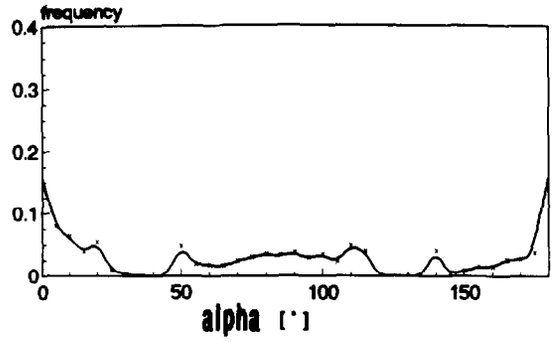

(b)

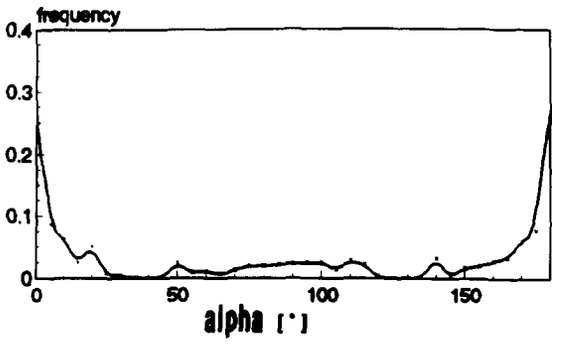

(c)

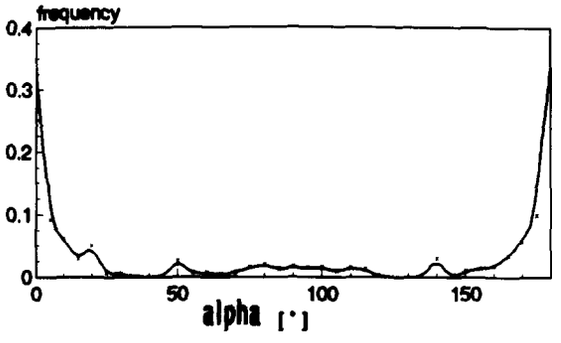

(d)

Fig. 7. Frequency distributions with respect to the angle α for the references (samples 1 and 3, (a) and (b)) and for the deformed states (samples 2 and 4, (c) and (d)).

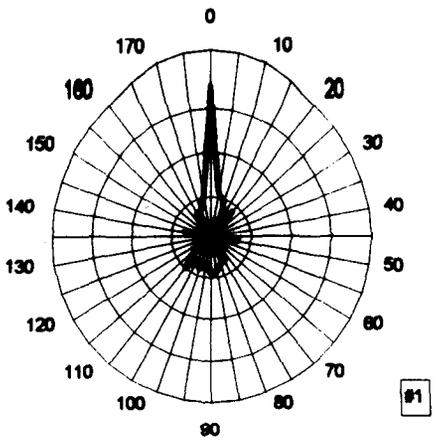

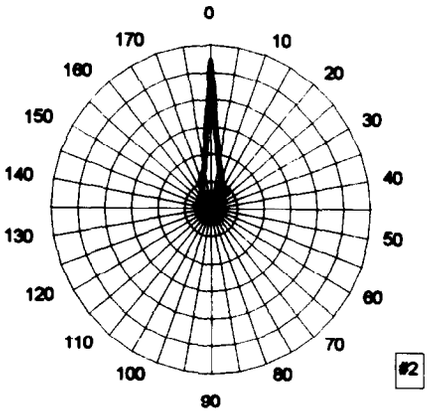

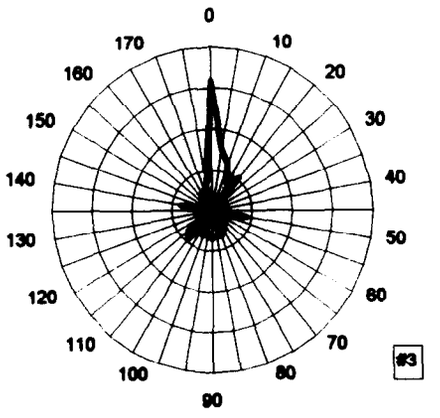

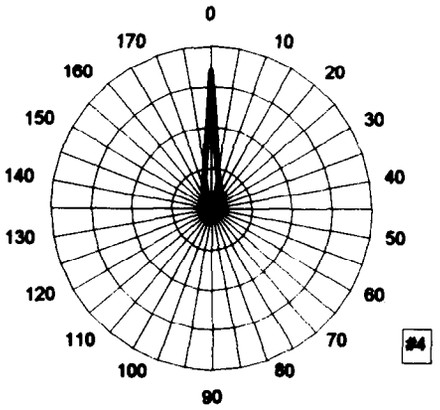

Fig. 8. Frequency distributions with respect to the angle α for the references (samples 1 and 3) and for the deformed states (samples 2 and 4) in a rose representation.

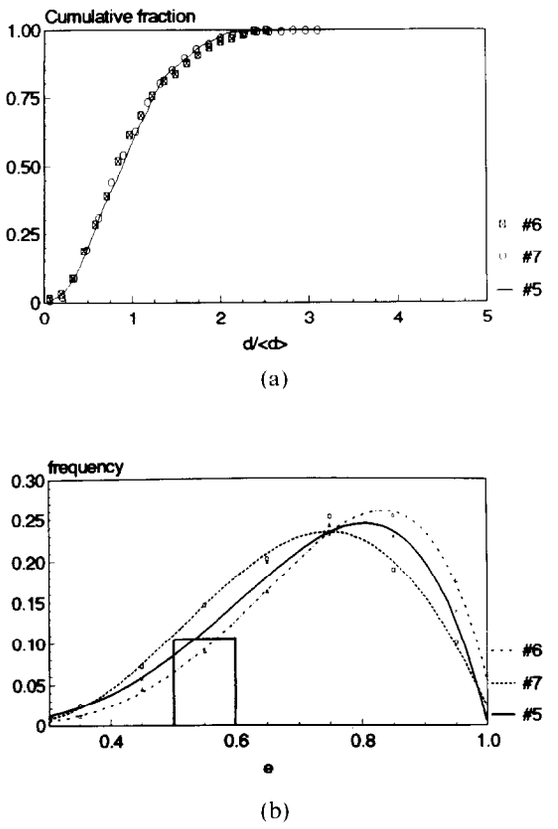

Fig. 9. Cumulative fractions with respect to the normalized equivalent grain diameter $d/\langle d\rangle$ (a) and frequency distributions with respect to the eccentricity e (b) for samples 5, 6 and 7. The value of the class has been drawn in (b).

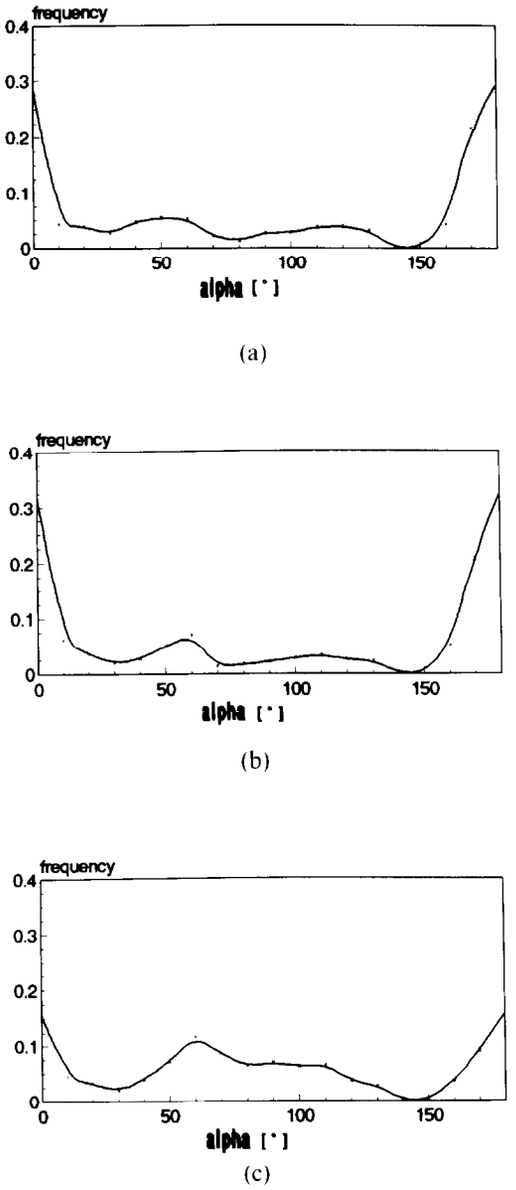

Fig. 10. Frequency distributions with respect to the angle α for samples (a) 5, (b) 6 and (c) 7.

In the curves corresponding to the two deformed states (Fig. 7(c) and (d)), it can be noticed that the number of grains for which α is close to 0° or 180° progressively increases with the deformation value, which is in agreement with the global analysis. This indicates that grains are preferentially orientated perpendicularly to the compressive stress σ.

These results are also displayed in a rose representation (Fig. 8). For the reference states (samples 1 and 3) grains are orientated in all directions. However, a maximum value of frequency is found close to 0°–180°. This indicates a slight preferential orientation of grains perpendicularly to P. This result was not clearly established by global analysis. As expected for the deformed specimens (samples 2 and 4) the majority of the grains are more preferentially orientated close to 0–180°.

4.2.2.2 Al grade (1·5 wt%). The cumulative distributions of the normalized equivalent grain diameter $d/\langle d\rangle$ (Fig. 9(a)) and the frequency curves of the eccentricity (Fig. 9(b)) (samples 6 and 7) seem not to be affected by the creep tests compared to the reference (sample 5). Taking into account the value of the class (0·1) for eccentricity, the slight shift of the modes for deformed samples is not significant compared to the reference state (Fig. 9(b)). On the other hand, if the distribution curves of α values for the three samples (5, 6 and 7, Fig. 10) are compared, sample 7 exhibits a different behaviour in terms of a decrease of the number of grains for which α is close to 0°–180°C. Consequently, grains of sample 7 (Fig. 10(c)), which is highly deformed, tend to be orientated in all directions.

The difference in distribution curves of α values for the three samples can be understood by the existence of a slight preferential orientation with respect to the stress P in the reference state (sample 5, Fig. 10(a)). Grains seem to have been reorientated with their large axes normal to the stress direction σ in sample 6 (Fig. 10(b)) while such orientated texture is not observed in sample 7 (Fig. 10(c)). These results for samples 5, 6 and 7 are also displayed in Fig. 11 in rose representations.

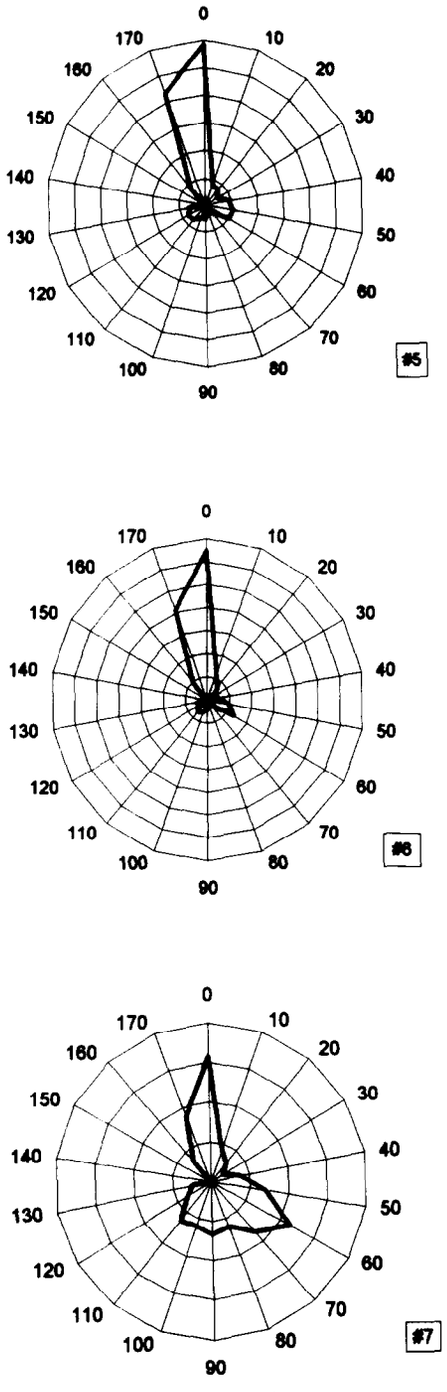

Fig. 11. Frequency distributions with respect to the angle α for samples 5, 6 and 7 in a rose representation.

5 Concluding Remarks

In this work, the microstructures of two SiC grades (0·3 and 1·5 wt% Al) have been characterized by automatic image analysis methods. Results of global and individual image analyses are in good agreement. The slight grain growth observed in annealed or deformed samples compared to the statistical scattering of the grain size does not allow a kinetic law of grain growth to be drawn in these experiments. The main results of the present work are the observation of a grain shape modification and a grain reorientation with respect to the external stresses which can be summarized as the following: grains of the deformed 0·3 wt% Al grade tend to flatten perpendicularly to the external stress. This was deduced from the eccentricity and α angle values (Table 1), showing that grains viewed in a cross-section containing σ can be described by an elliptic model. The other grade (1·5 wt%) exhibits a different microstructure evolution for a same deformation temperature range. Indeed, even for a high macroscopic deformation value, grains do not show any shape change after the creep test. Consequently, no texture formation could be found. All these results are important to understand the mechanical behaviour of these two SiC grades but further microstructural characterizations should be performed by TEM and microanalyses. Nevertheless, at this stage of the work, some hypotheses concerning the deformation mechanisms can be put forward:

(i) Al–SiC grade (0·3 wt%)
Different mechanisms could explain the fact that grain deformation follows approximately the specimen deformation as is demonstrated in this work (Fig. 3). A first mechanism is based on an important intragranular dislocation activity. SiC crystals exhibit mainly the hexagonal polytype (4H) and only one slip system (basal plane) is known to be the most activated.[13] This can induce the formation of a crystallographic texture. TEM observations[22] have effectively confirmed that grain boundaries tend to be parallel to the basal plane and normal to the stress direction. Moreover, an extended dislocation activity has also been analysed in detail in this deformed sample.[22] Consequently, an intragranular dislocation mechanism seems to be more favoured than a pure diffusion process which might also explain the grain shape change for this grade. Because no cavitation is observed, the grain boundary deformation has to be also accommodated either by an intergranular dislocation glide and/or by some diffusional matter transport via an intergranular film. Microanalyses and HREM experiments are still in progress to confirm effectively the presence of a thin intergranular film.

(ii) Al–SiC grade (1·5 wt%)
Compared to the preceding case, the mean grain size of the 1·5 wt% Al–SiC grade is now twice as small (Table 1). Because no grain shape change occurs the contribution of an intragranular dislocation activity to the overall deformation might be much lower than for the previous SiC grade. Moreover, as shown in Fig. 10, grains of the most deformed specimen (sample 7) are now dis-

tributed in all directions and have lost the slight preferential orientation observed by image analysis in the reference state (sample 5). These results suggest that an important rearrangement of grains has occurred during the deformation. All these data are in agreement with a superplastic-like behaviour for this grade as was previously suggested.[8] Because no cavitation is observed, stress accommodation could be relieved via diffusion and/or intergranular dislocation generation. Further observations in TEM should be performed to ascertain the exact mechanism.

Acknowledgement

One of the authors (M.L.D.) thanks the CNRS and the region of Basse Normandie for their financial support.

References

1. Krishnamachari, V. & Notis, M. R., Interpretation of high temperature creep of SiC by deformation mapping techniques. *Mat. Sci. Ing.*, **27** (1977) 83.
2. Wiederhorn, S. M., Ellis Roberts, D., Chuang, T. J. & Chuck, L., Damage-enhanced creep in a siliconized silicon carbide: Phenomenology. *J. Am. Ceram. Soc.*, **71** (1988) 602.
3. Moussa, R., Contribution à l'étude du comportement en fluage de matériaux SiC. Thesis, Caen, 1985.
4. Grathwohl, G., Reets, T. & Thummler, F., Creep of hot-pressed and sintered SiC with different sintering additives. *Sci. Ceram.*, **11** (1981) 425.
5. Farnsworth, P. L. & Coble, R. L., Deformation behavior of dense polycrystalline SiC. *J. Am. Ceram. Soc.*, **49** (1966) 264.
6. Francis, T. L. & Coble, R. L., Creep of polycrystalline silicon carbide. *J. Am. Ceram. Soc.*, **51** (1968) 115.
7. Djemel, A., Cadoz, J. & Philibert, J., Creep and fractures of engineering materials and structure, ed. B. Whilshire & D. R. J. Owen. Swansea Pineridge Press, 1981, p. 381.
8. Carry, C. & Mocellin, A., High temperature creep of dense fine grained silicon carbides. In *Materials Science Research, Vol 18*, eds. R. E. Tressler & R. C. Bradt. Plenum Press, New York, 1984, p. 391.
9. Carter, Jr, C. H., Davis, R. F. & Bentley, J., Kinetics and mechanisms of high-temperature creep in silicon carbide: I. Reaction-bonded. *J. Am. Ceram. Soc.*, **67** (1984) 409.
10. Carter, Jr, C. H., Davis, R. F. & Bentley, J., Kinetics and mechanisms of high-temperature creep in silicon carbide: II. Chemically vapor deposited. *J. Am. Ceram. Soc.*, **67** (1984) 732.
11. Lane, J.E., Carter, Jr, C. H. & Davis, R. F., Kinetics and mechanisms of high-temperature creep in silicon carbide: III. Sintered α-silicon carbide. *J. Am. Ceram. Soc.*, **71** (1988) 281.
12. Nixon, R. D. & Davis, R. D., Diffusion-accommodated grain boundary sliding and dislocation glide in the creep of sintered alpha silicon carbide. *J. Am. Ceram. Soc.*, **75**(7) (1992) 1786.
13. Lee, S. J. & Vicens, J., Interactions between Shockley dislocations and perfect screw dislocations with large Burgers vectors in high-temperature deformed α-SiC. *Phil. Mag. A*, **65** (1992) 551.
14. Demenet, J. L., Rabier, J. & Garem, H., Microstructure of sintered α-SiC deformed below 1000°C. In *6th M.S M. Inst. Phys. Conf. Ser. No. 100*, Section 5, Oxford, UK, 10–13 April 1989. p. 445.
15. Maeda, K., Suzuki, K., Fujita, S., Ichihara, M. & Hyodo, S., Defects in plastically deformed 6H SiC single crystals studied by transmission electron microscopy. *Phil. Mag. A*, **57** (1988) 573.
16. Fujita, S., Maeda, K. & Hyodo, S., Dislocation glide motion in 6H SiC single crystals subjected to high-temperature deformation. *J. Mater. Sci. Lett.*, **5** (1986) 450.
17. Burton, B., In *Diffusional Creep of Polycrystalline Materials*. Diffusion and Defects Monograph, Scrie Trans. Tech. Publ., 1977.
18. Kashyap, B. P. & Mukherjee, A. K., In *Superplasticity*, ed. B. Baudet & M. Suery, CNRS, Paris, 1985, p. 41.
19. Coster, M. & Chermant, J. L., *Précis d'analyse d'images*, 2nd edn. CNRS, Paris, 1989.
20. Serra, J., *Mathematical Morphology and Image Analysis*, Academic Press, New York, 1982.
21. Nauer, M., Microstructure et superplasticité de zircones yttriées. Thesis EPFL No. 996, Lausanne, Switzerland, 1992.
22. Duval-Riviere, M.L., Carry, C. & Vicens, J., Creep behaviour and microstructure evolution of hot-pressed alpha-silicon carbide deformed at high temperature. In *Third Euro-Ceramics*, Vol. 3, ed. P. Duran & J. F. Fernandez, FAENZA Editirice, Iberica S. L., 1993, p. 435.